
Evaluating the freeform modelling of point clouds by means of a test specimen

Corinna HARMENING, Gilles TEODORI, Hans NEUNER

TU Wien, Department of Geodesy and Geoinformation
Vienna, Austria
E-mail: corinna.harmening@tuwien.ac.at

Abstract

Areal measurement techniques like laser scanning require a change in engineering geodetic analysis strategies from a point wise perspective to an areal one. Usually, areal analysis strategies include a modelling of the acquired laser scanning point clouds in order to reduce the amount of data while preserving as much information as possible. A major advantage of the continuous geometric modelling is the description of the geometric shape and of its deformations by means of the parameters of the fitted surface. In this sense, freeform surfaces like B-splines have proven to be a suitable tool to model laser scanner point clouds. At TU Wien a test specimen with B-spline form was manufactured, forming the basis for the evaluation of the developed analysis strategies.

The aim of the paper is twofold: On the one hand the actual form of the test specimen is evaluated by means of a high-precision hand scanner and compared to the nominal one. On the other hand the well-known form of the specimen is used to compare the error characteristics of three laser scanners working according to different scanning principles.

Key words: B-Spline surfaces, form evaluation, laser scanning, point cloud modelling.

1 INTRODUCTION

Due to the establishment of terrestrial laser scanner in engineering geodesy, the respective analysis strategies change from pointwise approaches to areal ones. Freeform surfaces like B-splines have proven to be a suitable tool to model laser scanner point clouds and thus to form the basis for an areal data analysis. However, the determination of B-spline surfaces based on laser scanning point clouds is not straightforward, but requires sophisticated algorithms to determine all parameter groups, which characterize a B-spline surface, in a satisfying manner. To evaluate those algorithms, previously, simulated data sets were used (Kauker et al. 2017). However, these simulation studies have shown that the measuring process is still not fully understood, resulting in simulated data sets which do not represent reality in an appropriate way. For this reason, a test specimen was manufactured based on a known B-spline model. On the one hand, this test specimen allows the evaluation of the developed B-spline-models based on realistic data; on the other hand, it provides the opportunity to investigate the uncertainty budget of laser scanner by comparing the determined shape to the nominal one. The results can be used to improve existing simulation models.

TS 7 – Terrestrial Laser Scanning

Before the specimen can be used to verify the algorithms' results, a form evaluation has to be performed, guaranteeing that the actual form of the specimen corresponds to the theoretical model on which the manufacturing process was based. This paper presents the results of this form evaluation, which is realized by means of a high-precision hand-held scanner.

Afterwards, the well-known form of the specimen is used to investigate laser scanner with respect to their error characteristics. This paper focuses on the comparison of three laser scanner distinguishing themselves in their measuring principle.

2 B-SPLINE-BASED POINT CLOUD MODELLING

A B-spline surface $S(u, v)$ of degree p and q is defined by (Piegl, L. A. & Tiller, W. 1997):

$$S(u, v) = \sum_{i=0}^m \sum_{j=0}^n N_{i,p}(u) N_{j,q}(v) P_{ij} \quad , \text{ with: } u, v = [0, \dots, 1]. \quad (1)$$

A surface point $S(u, v)$ is thus expressed as the weighted average of the $(n+1)*(m+1)$ control points P_{ij} . The corresponding weights are defined by the B-spline basis functions $N_{i,p}(u)$ and $N_{j,q}(v)$ which can be computed recursively by means of the Cox-de-Boor-algorithm (Cox, M.G. (1972), de Boor, C. (1972)).

Two knot vectors $U = [u_0, \dots, u_r]$ and $V = [v_0, \dots, v_s]$ split the B-spline's domain into knot spans. Hence, when estimating a best-fitting B-Spline surface, a variety of unknown parameters has to be determined, generally leading to a nonlinear adjustment problem. Usually, a linear estimation problem which determines only the control points' positions is targeted. For this reason, the remaining parameters are either set (according to Piegl, L. A. & Tiller, W. (1997) the choice of $p = 3$ and $q = 3$ is generally accepted) or determined independently of the control points' estimation (e.g. knot vectors: Schmitt, C. & Neuner, H. (2015), Bureick, J. et al. (2016)); surface parameters: Harmening, C. & Neuner, H. (2015); numbers of control points: Harmening, C. & Neuner, H. (2016), Harmening, C. & Neuner, H. (2017)).

3 TEST SPECIMEN AND MEASURING CONFIGURATIONS

3.1 TEST SPECIMEN WITH B-SPLINE FORM

The development of algorithms to determine the B-spline's parameter groups requires a validation. For this reason, based on a known B-spline model, a test specimen was milled out of a massive aluminium block of 40 cm x 40 cm x 20 cm. In order to improve the reflection properties, the surface was sandblasted afterwards using precious corundum with a grain size of 600 – 850 μm . An allocation of the known surface parameters (u, v) to the measured point cloud requires a known orientation of the test specimen relative to the laser scanner. For this reason, ten reference points are evenly distributed along the surface's boundary: Five of them (green circles in Fig. 1) are marked by a cross, which can be measured by means of a tacheometric measuring system (TMS) and the other five (blue circles in Fig. 1) provide the opportunity to attach a corner cube reflector, allowing a laser tracker measurement. The nominal coordinates of the crosses' and the corner cubes' centres (in the planning coordinate system) were determined during the manufacturing process.

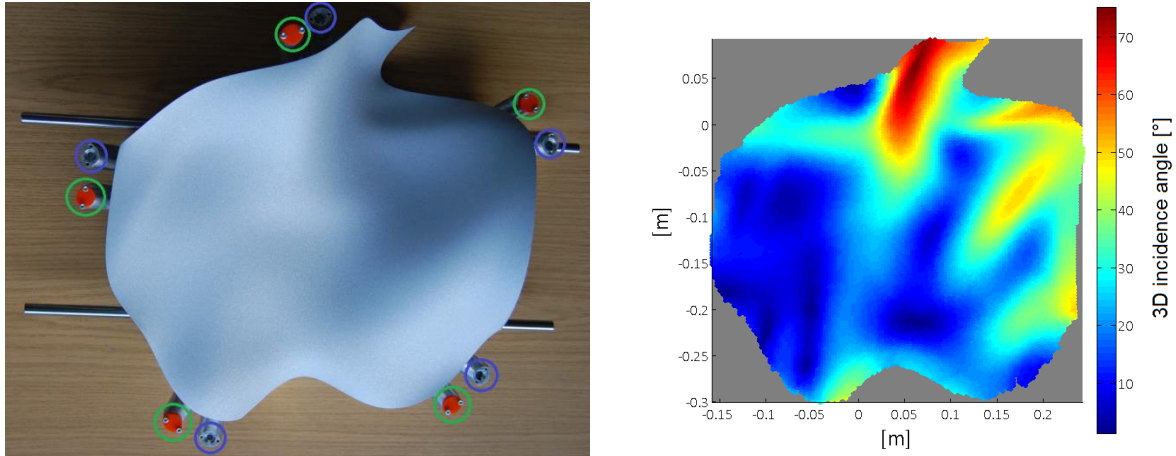


Fig. 1 Test specimen in B-spline form with reference points for the TMS (green circles, they are covered by protective caps) and for the laser tracker (blue circles) (left), 3D incidence angles of the laser beam (right).

A photo of the test specimen can be seen in figure 1 (left). Due to the choice of the B-spline's parameters, the test specimen has an undulating surface, leading to a variety of incidence angles as can be seen in figure 1 (right). Depicted are the 3D incidence angles resulting from a measuring configuration where the specimen's ground plane is approximately perpendicular to the scanner's horizontal collimation axis, meeting the specimen at (0,0).

3.2 FORM EVALUATION

In order to guarantee that the specimen's actual form does not differ significantly from the planned one, the test specimen is scanned by means of a high precision hand-held scanner, providing an accuracy of more than an order of magnitude higher than classical terrestrial laser scanners do. The orientation of the hand-held scanner as well as of the test specimen is determined by means of a laser tracker. Based on the five pairs of corresponding reference points, which are known in the measuring coordinate system (laser tracker measurements) as well as in the planning coordinate system (manufacturing process), a high-accurate transformation of the point cloud into the planning coordinate system (CAD-CS, figure 3) and, as a consequence, a direct comparison of the CAD model with the measured point cloud is possible.

Already a visual comparison reveals discrepancies between the measured point cloud and a generated point cloud describing the nominal surface. Taking into account that the measuring of the reference points' nominal coordinates was realized independently of the milling process, the assumption that these discrepancies are caused by a misalignment of the reference points relative to the B-spline surface is justified. This misalignment results in an incomplete orientation. For this reason, the measured point cloud is post-oriented by means of the Iterative Closest Point (ICP) algorithm (Besl, P.J. & McKay, N. D. 1992). In figure 2 the translations of each measured point caused by the ICP algorithm can be seen. In all three coordinate directions the amount of the translation clearly exceeds the accuracy of the hand-held scanner and hence can be regarded to be significant. At this point, a spatial distribution of the translations is spared, as the general displacement rather than the translations' distribution with respect to the surface is of interest.

While the application of the ICP algorithm improves the relative orientation of the measured point cloud with respect to the nominal one, it deteriorates the discrepancies between the

measured reference points and the nominal ones as can be seen in table 1, showing the respective discrepancies before and after applying the ICP algorithm: The very small discrepancies between the reference points before applying the ICP algorithm reveal a consistent relative position of the reference points to each other, whereas the significantly larger discrepancies after applying the ICP algorithm indicate a misorientation of the reference points relative to the surface. Applying the transformations given by the ICP to the coordinates of the reference points in the manufacturing system provides new reference coordinates which will be used to orientate the specimen in future.

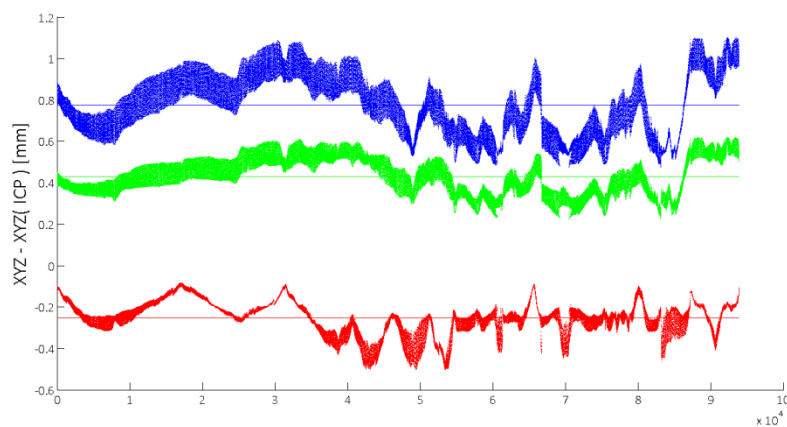


Fig. 2 Translation of each point of the point cloud caused by the ICP algorithm (red: x-coordinate, green: y-coordinate, blue: z-coordinate)

Discrepancies of the reference points [mm]		
Before using the ICP:		
ΔX	ΔY	ΔZ
0,001	0,018	0,005
0,006	-0,001	-0,012
0,005	-0,009	0,002
-0,012	-0,008	0,004
After using the ICP:		
ΔX	ΔY	ΔZ
-0,089	0,419	0,822
-0,291	0,283	0,516
-0,479	0,358	0,555
-0,409	0,562	0,915

Tab. 1 Discrepancies between the measured reference points and the nominal ones.

3.3 MEASURING CONFIGURATIONS

The test specimen was captured by three different measurement instruments.

Tab. 2 Measurement performances of the used laser scanner

	TLS1	TLS2	TLS3
Type	Scanning total station	Laser scanner	Laser scanner
Measuring principle	Time of flight	Phase-shift	Time of flight
distance accuracy	2 mm + 2 ppm	0,4 mm (10 m)	8 mm (150 m)
angular accuracy	1'' (0,3 mgon)	125 mrad	0,0015°
beam divergence	≈ 0,4 mrad	< 0,3 mrad	0,3 mrad
Typical measuring distance	10 – 100 m	10 – 100 m	100 m – 2 km

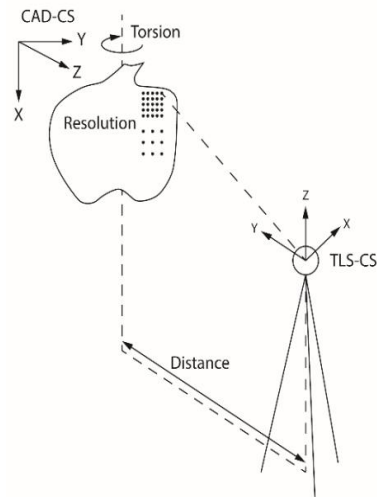


Fig. 3 Measuring configuration

The TLS1 is a scanning total station, whereas the TLS2 and TLS3 are ordinary laser scanners. Some of the laser scanners characteristics and performances are described in table 2.

During the measurements, the specimen was held by a support structure and positioned on a stable table in front of the laser scanner (cf. figure 3). In order to investigate the error characteristics of the laser scanner, the specimen was scanned under different measurement configurations. These configurations were created by varying the torsion angle, the sampling resolution and the measurement distance (cf. figure 3). By fixing two and varying one of these three settings, series of datasets have been acquired. The analysis of these series can be used to determinate the influence of the varying setting on the measurements as well as to compare the laser scanners' performances.

The acquired datasets have been measured in the respective right-handed coordinate system (TLS-CS) of the laser scanners. In order to make the evaluated datasets comparable to the nominal form, the datasets need to be transformed in a project coordinate system (CAD-CS), which is realized by means of the reference points.

4 COMPARISON OF DIFFERENT LASER SCANNER

The well-known form of the laser scanner can now be used to investigate and compare those laser scanners with respect to their error characteristics. For this reason, the control points of B-spline surfaces are estimated based on the measured point clouds. The remaining B-spline's parameter groups (cf. section 2) are set to the nominal values. Based on the estimation results, the residuals of the form fitting are investigated, and the estimated control points are compared to the nominal ones.

4.1 RESIDUALS OF THE FORM FITTING

Figure 4 shows the residuals' histograms of the B-spline estimation resulting from comparable measuring configurations of the three laser scanner introduced in section 3.2. As in general the residuals are assumed to be normally distributed, a density function of the normal distribution is fitted through the histograms (black curve).

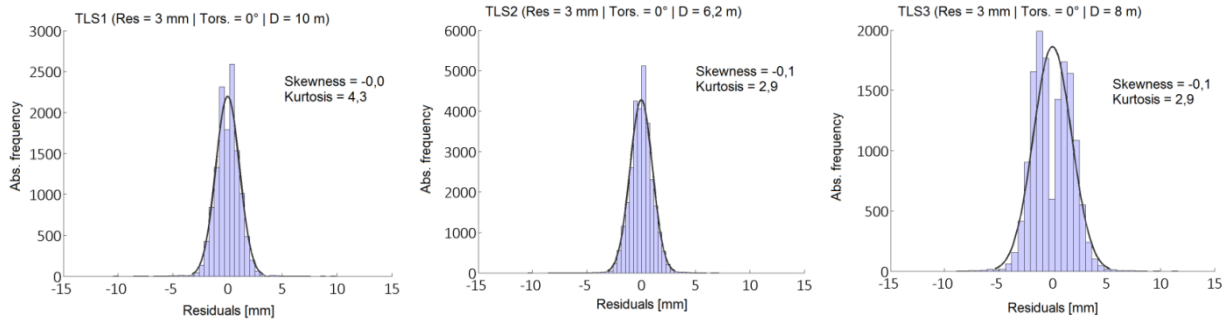


Fig. 4 Histograms of the residuals (blue) and fitted normal density functions (black curve) for TLS1 (left), TLS2 (middle) and TLS3 (right).

The histograms of the laser scanner TLS1 and TLS 2 show a high level of visual agreement with the respective density functions, whereas the histogram of TLS3 describes a bimodal distribution of the residuals and, as a consequence, it is not approximated sufficiently by the fitted density function.

For further investigations, the first four statistical moments of the residuals’ distribution are computed and listed in table 3.

Tab. 3 Statistical moments of the residuals’ histograms

	Mean [mm]	Median [mm]	Std. [mm]	Skewness	Kurtosis
TLS1	0,00	0,04	1,1	-0,03	4,28
TLS2	0,00	0,02	1,0	-0,11	2,88
TLS3	0,01	-0,24	1,8	0,13	0,42

Comparing the statistical moments of the three scanners, the mean values as well as the skewness do not show conspicuous differences: All three histograms are symmetric and centred at zero. The differences between the residuals of TLS3 compared to the other two scanners become apparent in the standard deviations as well as in the kurtosis: The standard deviations indicate a considerably larger variation of the residuals of TLS3 than of the other two scanners, whereas the kurtosis indicates the histogram of TLS3 to be closer to a mesokurtic distribution than the other two.

A comparison of the empirical determined standard deviations to the manufacturer’s specifications in table 1 reveals that TLS1 and TLS3 perform better than expected. The opposite is true for TLS2: Although the empirical standard deviations are the smallest compared to TLS1 and TLS3, it is more than twice as large as the manufacturer states. However, it has to be noted that the results of TLS3 have to be viewed carefully: Being a long-range scanner, the realised measurement distances between 3 and 10 m are not the typical distances, this scanner is used for.

To evaluate if the residuals are normally distributed, the normality test according to Pelzer, H. (1980) is performed: If the test statistics $T_1 = c_1\sqrt{n/6}$ and $T_2 = c_2\sqrt{n/24}$, with n being the sample size, c_1 being the skewness and c_2 being the kurtosis, exceed in absolute value the quantile $X_{1-\alpha/4}^2$, the hypothesis that the sample is normally distributed has to be discarded. In table 4 the results of the normality test using a significance level of $\alpha = 5\%$ are listed.

Tab. 4 Test statistics and quantiles for the normality test according to Pelzer, H. (1980).

	T_1	T_2	$X_{1-\alpha/4}^2$
TLS1	-1.3895	99.1200	6.2385
TLS2	-7.7071	100.8925	6.2385
TLS3	6.3828	10.3107	6.2385

In all three cases the test statistics T_2 indicates a kurtosis being significantly larger than the kurtosis of a normal distribution. The same applies for the skewness in case of the data sets of TLS2 and TLS3. As a consequence, neither of the sets of residuals can be assumed to be normally distributed.

4.2 COMPARISON OF THE POINT CLOUDS TO THE NOMINAL FORM

The well-known form of the test specimen allows a comparison of the estimated control points to the nominal ones and, as a consequence, it allows conclusions about the quality with which the three laser scanner acquire the test specimen. In figure 5 the discrepancies of the estimated control points to the nominal ones are represented for all three laser scanner and two measuring configuration each, differing by the scanning resolution. In all three cases the discrepancies decrease when increasing the resolution. Next to the well-known relationship between the sample size and the approximation quality, the spot size can be used to interpret the results: In scanning distances of 6-8 m the spot sizes of TLS1 and TLS2 are about 3 mm. As a consequence, in the measuring configurations with the higher resolution, the laser spot of neighbouring measurements superimposes, leading to an increase of correlations.

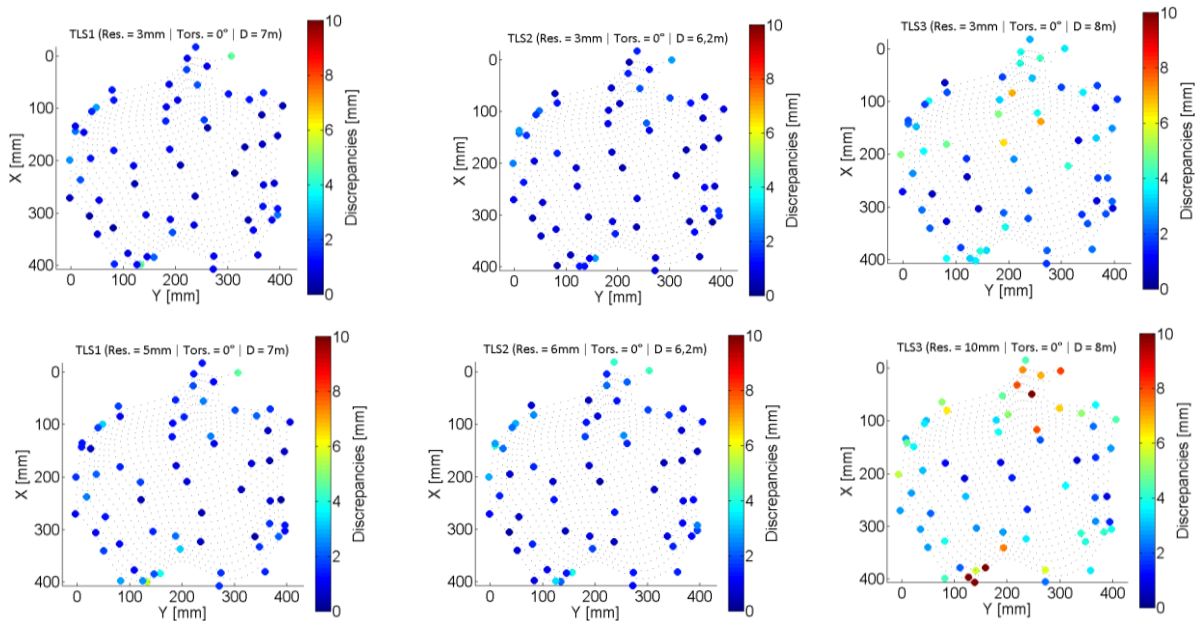


Fig. 5 Discrepancies between the estimated control points and the nominal ones.

The comparison of the three laser scanner shows similar results of TLS1 and TLS2: The discrepancies vary around zero and take on maximal values of about 2 mm at a scanning resolution of 3 mm and maximal values of about 5 mm at a scanning resolution of 5 and 6 mm respectively. It is conspicuous that these maximal values occur in the boundary regions of the test specimen. As indicated by the results of section 4.1, TLS3 performs worse than the other two scanners as the discrepancies are significantly larger. However, it has to be taken into

account that TLS3 is designed for much larger measuring distances and that these results allow no conclusion about the scanner's performance in case of long ranges.

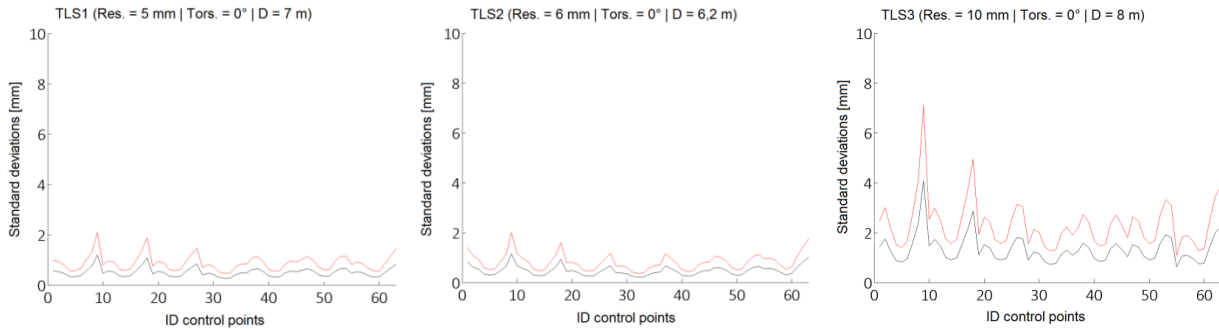


Fig. 6 Standard deviations (black) and point error by Helmert (red) of the estimated control points for TLS1 (left), TLS2 (middle) and TLS3 (right).

These findings are supported by figure 6, depicting the standard deviations of the three coordinates (red curve, equal for each coordinate) as well as the point error by Helmert (black curve). Analogously to the discrepancies of the control points, the standard deviations resulting from the measurements of TLS1 and TLS2 take very similar values, whereas the standard deviations resulting from TLS3 are significantly larger.

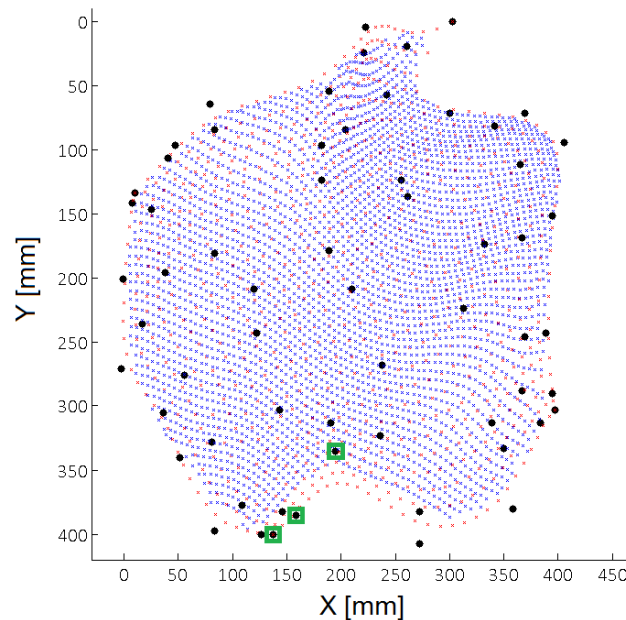


Fig. 7 Position of the control points with conspicuous standard deviation

However, all three figures have a conspicuous pattern in common, showing larger standard deviations of every ninth control point than of the remaining ones, especially at the control points 9, 18 and 27. In order to investigate this behaviour, in figure 7 one of the measured point clouds (blue points), a nominal point cloud (red points) and the estimated control points (black points) are depicted. The conspicuous control points 9, 18 and 27 are marked by means of green rectangles. As can be seen, these control points are located at the lower edge of the test specimen which was captured incompletely by the laser scanner. The location of the control points leads to a comparatively small number of observations supporting the estimation of those points which is reflected by the comparatively high precision.

5 CONCLUSION

The development of B-spline based areal analysis strategies requires a possibility to validate the respective results. For this reason, at TU Wien a test specimen with B-spline form was manufactured. In this paper, the actual form was evaluated by means of a high-precision hand-held laser scanner revealing a misorientation between the surface and the reference points serving to determine the relative orientation between test specimen and laser scanner. Using improved reference points, the test specimen was used to compare the error characteristics of three laser scanner, distinguishing themselves by means of their measuring principle. The investigations revealed comparable performance qualities in case of a scanning total station and a TLS working according to the phase-shift principle. The long-range scanner using the time-of-flight principle performs significantly worse, caused by measuring distances which are significantly smaller than the typical operation range.

ACKNOWLEDGEMENT

The presented paper shows results developed during the research project "Integrierte raumzeitliche Modellierung unter Nutzung korrelierter Messgrößen zur Ableitung von Aufnahme Konfigurationen und Beschreibung von Deformationsvorgängen" (IMKAD) (1706-N29), which is funded by the Austrian Science Fund (FWF).

The measurements were carried out in cooperation with the Institute of Engineering Geodesy of the University of Stuttgart.

REFERENCES

- Besl, P. J. - McKay, N. D. 1992. A method for registration of 3-D shapes. In *IEEE Transactions on Pattern Analysis and Machine Intelligence*, 1992, vol. 14, no. 2, pp. 239–256.
- Bureick, J. - Alkhatib, H. - Neumann, I. 2016. Robust Spatial Approximation of Laser Scanner Point Clouds by Means of Free-form Curve Approaches in Deformation Analysis. In *Journal of Applied Geodesy*, 2016, vol. 10, no. 1, pp. 27-35.
- Cox, M. G. 1972. The Numerical Evaluation of B-Splines. In *IMA Journal of Applied Mathematics*, 1972, vol. 10, no. 2, pp. 134-149.
- de Boor, C. 1972. On calculating with B-splines. In *Journal of Approximation Theory*, 1972, vol. 6, no. 1, pp. 50-62.
- Harmening, C. - Neuner, H. 2015. A constraint-based parameterization technique for B-spline surfaces. In *Journal of Applied Geodesy*, 2015, vol. 9, no. 3, pp 143-161.
- Harmening, C. - Neuner, H. 2016. Choosing the Optimal Number of B-spline Control Points (Part 1: Methodology and Approximation of Curves). In *Journal of Applied Geodesy*, 2016, vol. 10, no. 3, pp 139-157.
- Harmening, C. - Neuner, H. 2017. Choosing the optimal number of B-spline control points (Part 2: Approximation of surfaces and applications). In *Journal of Applied Geodesy*, 2017, vol. 11, no. 1, pp. 43-52.

- Kauker, S. - Harmening, C. - Neuner, H. - Schwieger, V. 2017. Modellierung und Auswirkung von Korrelationen bei der Schätzung von Deformationsparametern beim terrestrischen Laserscanning. In Lienhart, W. (ed.): Ingenieurvermessung 17. Beiträge zum 18. Internationalen Ingenieurvermessungskurs Graz, 2017. Wichmann Verlag, Berlin/Offenbach, pp. 321-336.
- Pelzer, H. 1980. Geodätische Netze in Landes- und Ingenieurvermessung. Vorträge des Kontaktstudiums Februar 1979 in Hannover. Stuttgart: Wittwer (Vermessungswesen bei Konrad Wittwer, Bd. 5).
- Piegl, L. A. - Tiller, W. 1997. The NURBS book. 2nd edition. Berlin and New York: Springer (Monographs in visual communications).
- Schmitt, C. - Neuner, H. 2015. Knot estimation on B-Spline curves. In Österreichische Zeitschrift für Vermessung und Geoinformation (VGI), 2015, vol. 103, no. 2+3, pp. 188-197.